Biophysical Journal, Volume *117*

Supplemental Information

Mechanical Point Loading Induces Cortex Stiffening and Actin Reorganization

Jinrong Hu, Shenbao Chen, Wenhui Hu, Shouqin Lü, and Mian Long

Mechanical point loading induces cortex stiffening and actin reorganization

Jinrong Hu[1,2], Shenbao Chen[1,2], Wenhui Hu[1,3], Shouqin Lü[1,2†], and Mian Long[1,2†]

[1]Center of Biomechanics and Bioengineering, Key Laboratory of Microgravity (National Microgravity Laboratory), Beijing Key Laboratory of Engineered Construction and Mechanobiology, and CAS Center for Excellence in Complex System Mechanics, Institute of Mechanics, Chinese Academy of Sciences, Beijing, China.

[2]School of Engineering Science, University of Chinese Academy of Sciences, Beijing, China.

[3]Immune Cells and Antibody Engineering Research Center, Guizhou Province/Key Laboratory of Biology and Medical Engineering, Guizhou Medical University, Guiyang, China.

Supplementary Figures and Figure Captions

Figure S1

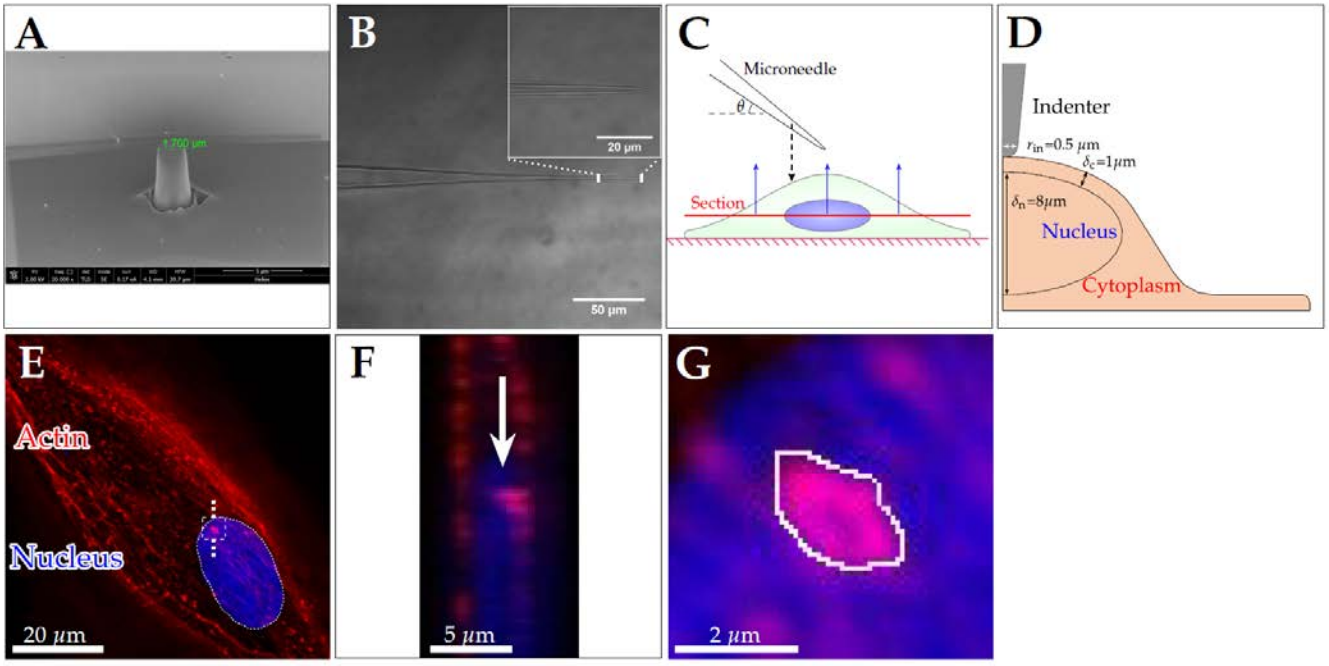

Figure S1. Schematics of point loading approach to the cell from the top of the nucleus, the geometry model for simulations and data collection of local actin fluorescence intensity in a cell. (*A*) Typical SEM image presented the truncated cylinder CSG-10 probe with a height of 3-4 μm and a tip diameter of 1.5-2 μm, which was used to point load the cell with assigned force using AFM assay. (*B*) Borosilicate glass microneedle was used to point load the cell. Zoomed in the insert showed the tip of needle with a radius around 1.5 μm. (*C*) Protocols of collecting the fluorescent information and point loading the cell using either microneedle or AFM tip (only shown with microneedle for clarity). Here the cell was segregated into upper and lower regions (segmented at the middle plane of the nucleus in the cross section) and only fluorescence in the upper region (one above the red line) was collected to exclude the potential interference originating from the basal fluorescence of stress fibers in the lower region. Microneedle loading path was depicted using black dashed downward arrow (indentation depth 3-5 μm). $\theta \approx 45°$ for the needle or 90° for AFM tip. (*D*) Schematic of the geometry model for simulations. r_{in} denoted the radius of AFM tip, δ_c the thickness of cytoplasm (or cortex) above the nucleus, and δ_n the dimension of the nucleus. (*E-G*) When loading the cell using AFM probe depicted in (*A*), local actin intensity enhancement in a typical HF cell could be evidently visible at the loading site (*red* spot inside the *white* dashed box in (*E*), as magnified in (*F*) using the *white* arrow and further magnified in (*G*) with *white* ring encircled. Local actin intensity enhancement was also visualized from side view along the *white* dotted line (dotted line within the dashed box was omitted for clarity) in (*E*), as magnified in (*F*). The extent of the local actin intensity enhancement was assessed using the ratio of mean fluorescence intensity in the white ring I_{ROI} (*G*) to average fluorescence intensity above the nucleus I_N (to exclude the potential interference from peripheral, strong stress fibers), that is, $I_{Relative} = I_{ROI}/I_N$.

Figure S2

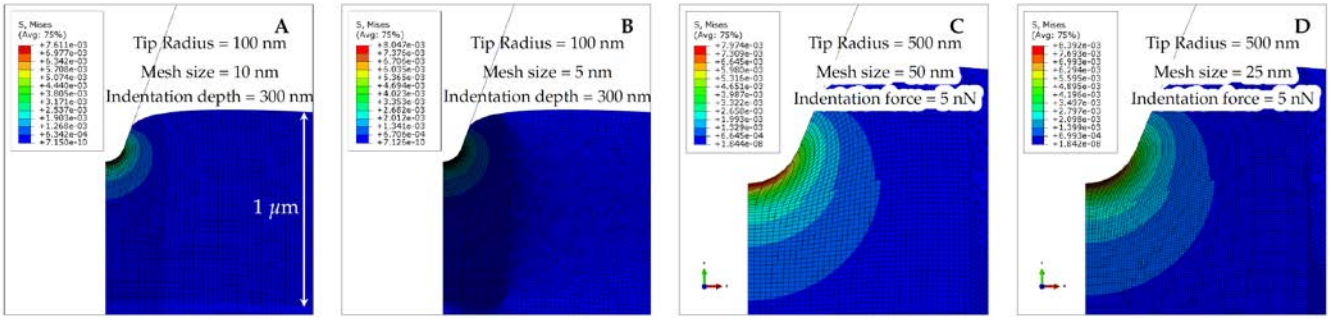

Figure S2. Computational modeling of indentation test using sharp tips with 100/500-nm radii. von Mise stress distributions were presented with mesh size of 10 nm (*A*) and 5 nm (*B*) upon 0.2 nN loading/300-nm indentation and with mesh size of 50 nm (*C*) and 25 nm (*D*) upon 5 nN loading. The converged results can only be obtained in loading of 0.2 nN/300-nm for 100-nm tip radius, which yields far smaller force value than the applied force of 5 nN. That is why the tip radius 500 nm was chosen for the simulations of the sharp-ended probe.

Figure S3

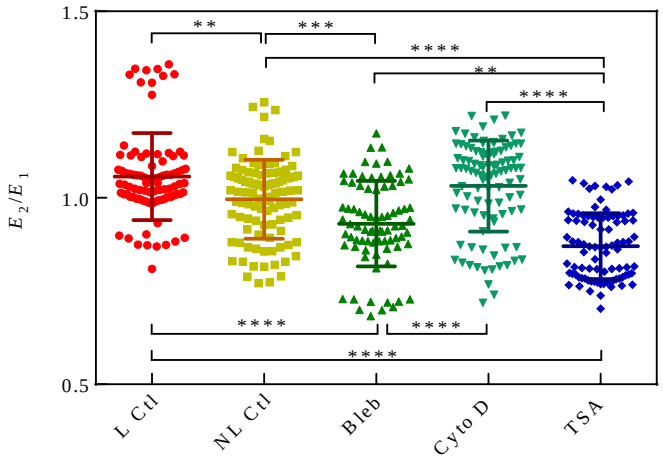

Figure S3. Statistics of E_2/E_1 ratios for all the groups. Each ring has one E_2/E_1 ratio and there are 10 data points for each cell and 9, 10, 8, 10 and 9 cells for *L Ctl*, *NL Ctl*, *Bleb*-, *Cyto D*- and *TSA*-treated groups, respectively. *L Ctl*, loading control; *NL Ctl*, non-loading control. **, $p < 0.01$, ***, $p < 0.001$, ****, $p < 0.0001$.

Figure S4

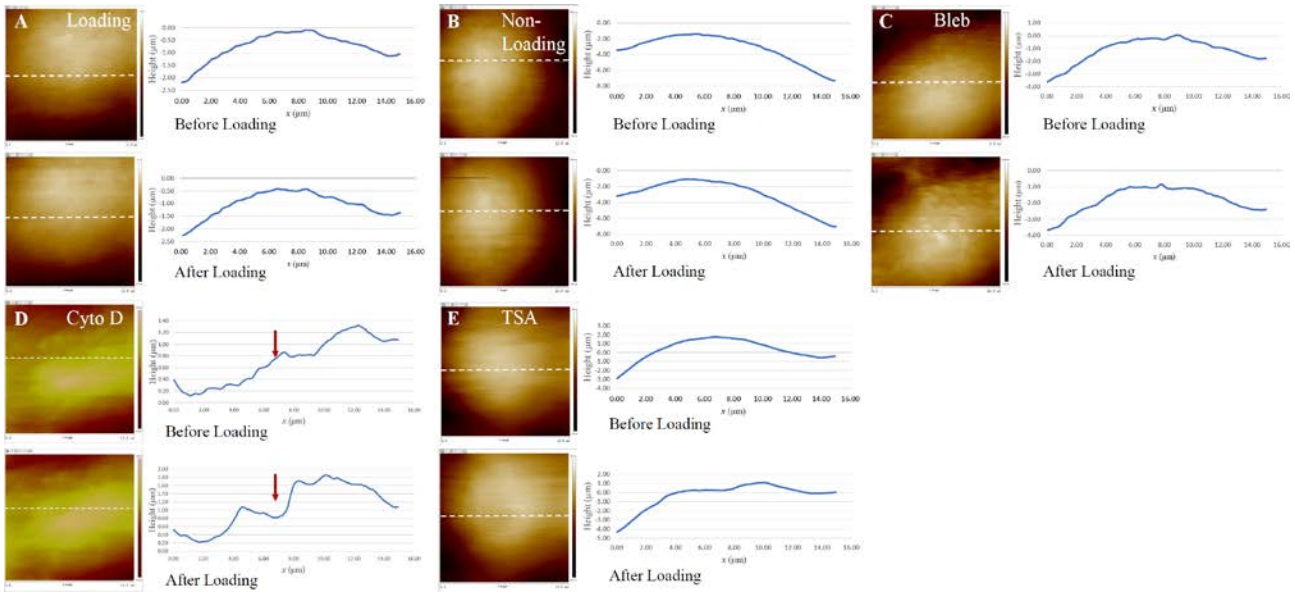

Figure S4. Representative height profiles across loading centers for *Loading* (*A*), *Non-Loading* (*B*), *Bleb*- (*C*), *Cyto D*- (*D*) and *TSA*-treated (E) groups. Both scanning image (*left*) and corresponding height profile (*right*) along the section crossing loading centers (*white dashed line*) were presented in each panel. The *red arrows* in panel (*D*) denoted the unrecoverable deformation of the cell upon Cyto D treatment.

Figure S5

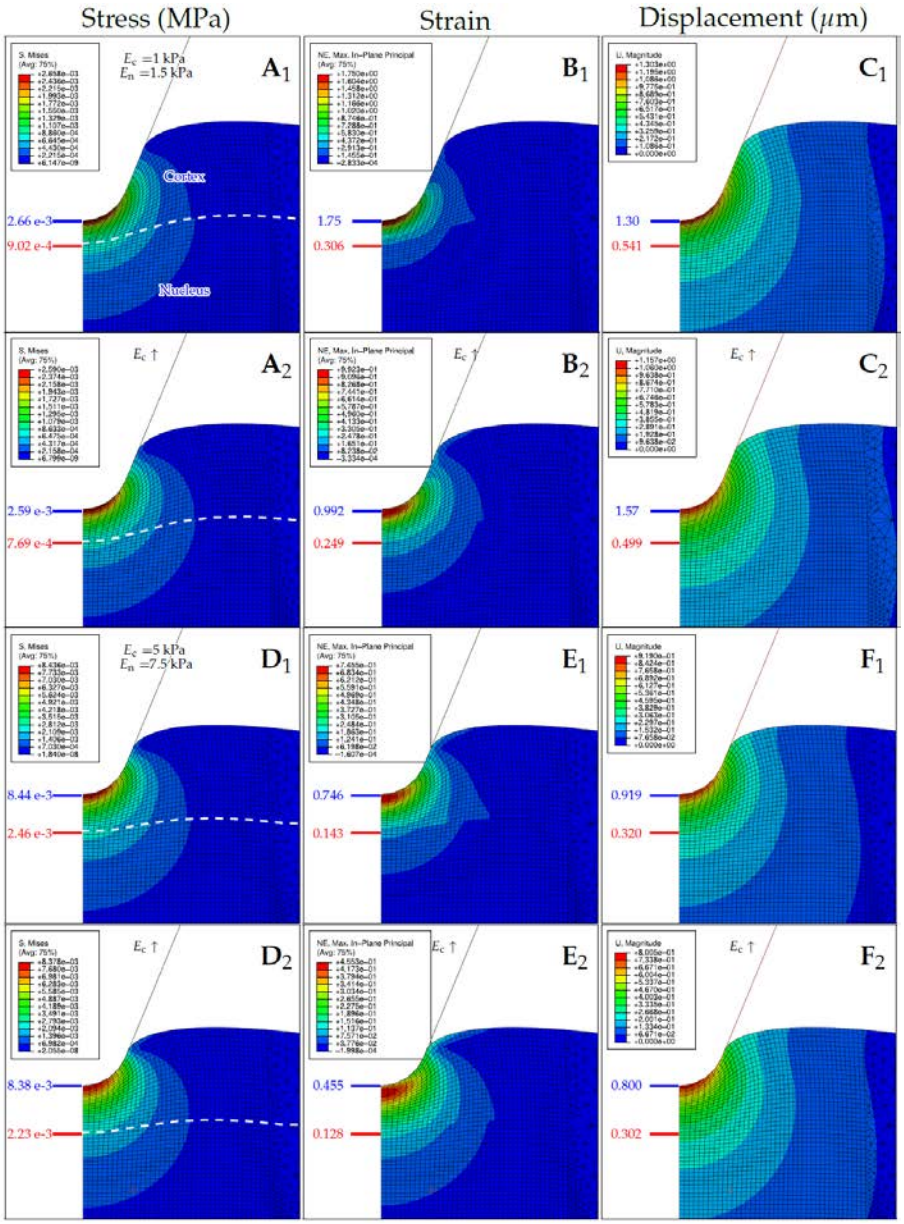

Figure S5. Parametric analyses of mechanical modeling. (*A*-*F*) Distribution of von Mises stress σ_{von}, maximum strain ϵ and magnitude of deformation *U*. In (A_1-C_1), E_c = 1 kPa and E_n = 1.5 kPa (subscript '*c*' denotes the cytoplasm and '*n*' the nucleus) were used and corresponding results of cortex stiffening were shown in (A_2-C_2) with $E_c' = 1.35\ E_c$ ($E_c \uparrow$) and E_n = 1.5 kPa. In (D_1-F_1), E_c = 5 kPa and E_n = 7.5 kPa were used and corresponding results of cortex stiffening were shown in (D_2-F_2) with $E_c' = 1.35\ E_c$ ($E_c \uparrow$) and E_n = 7.5 kPa. *Blue* lines and values denoted the maximum σ_{von}, ϵ and *U* of cortex, and *red* lines and values were for the nucleus. From (*A*-*C*) (with E_c = 1 kPa, E_n = 1.5 kPa, and loading force of around 2 nN), the maximum σ_{von}, ϵ and *U* had 2.6%, 43.3% and 10.8% decrease for cell cortex, and 14.7%, 18.6% and 7.8% decrease for the nucleus, respectively. From (*D*-*F*) (with E_c = 5 kPa and E_n = 7.5 kPa, and loading force of 5 nN), the maximum σ_{von}, ϵ and *U* yielded 0.7%, 39% and 12.9% decrease for cell cortex, and 9.3%, 10.5% and 5.6% decrease for the nucleus, respectively (details in Table 1).

Figure S6

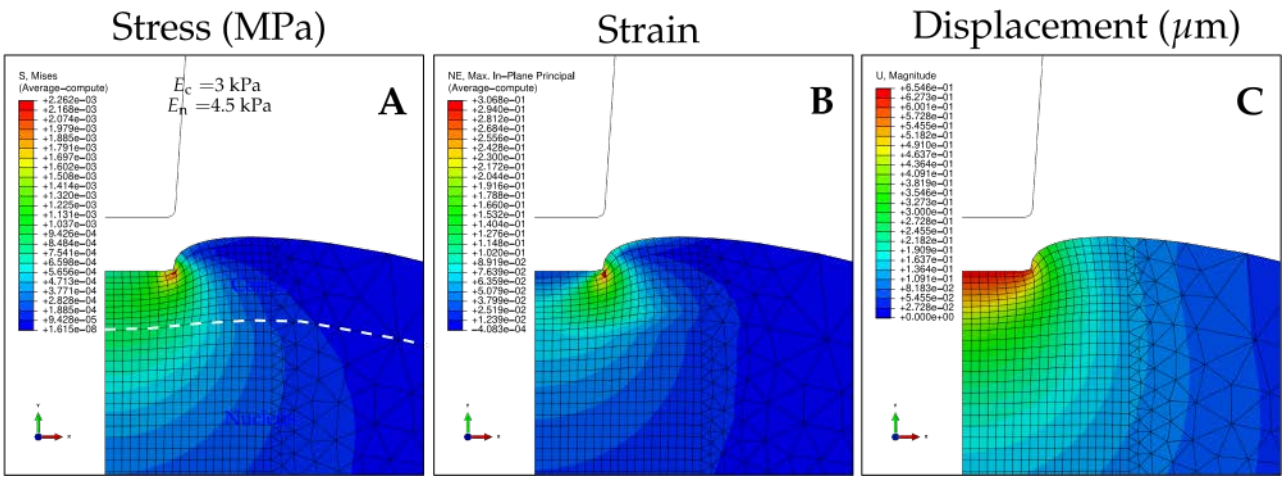

Figure S6. Stress, strain and deformation fields simulations upon flat-ended cylinder-like probe induced indentation (tip diameter was set to be 1.7 μm as in Fig. S1 *A*). Stress field revealed that geometrical jump at the periphery of the tip (a ring when considering the model as axisymmetric) could incur large increase of stress (*A*) and strain (*B*) even though the change in displacement showed a different pattern (*C*). The loading force was 5 nN.

Figure S7

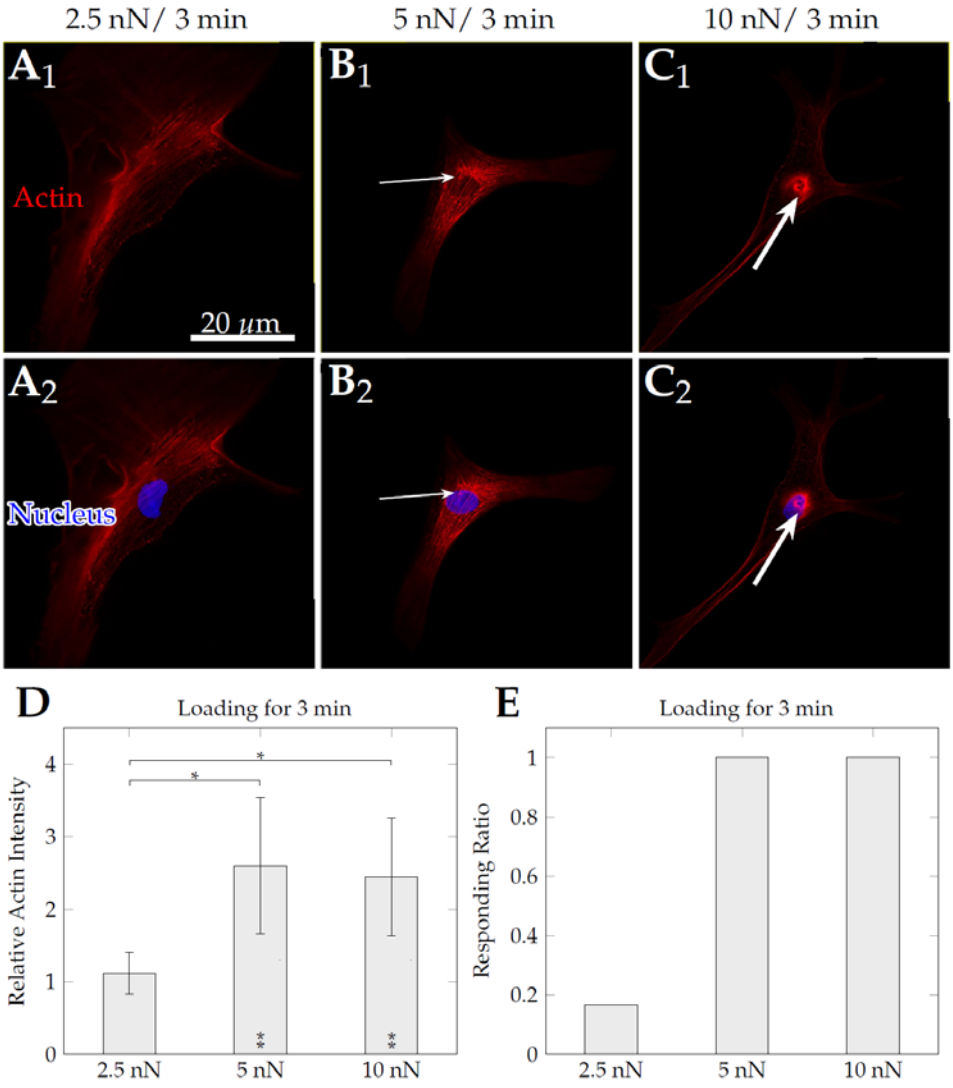

Figure S7. Loading force dependence of local actin intensity enhancement after point loading for HF cells upon AFM assay. (2.5, 5 and 10 nN) / 3 min were used to load HFs ((A_1-C_1) for actin (*red*) alone and (A_2-C_2) with nucleus (*blue*) presented). *White* arrows indicated the loading sites and local actin intensity enhancement were captured in (5, 10) nN / 3 min but not in 2.5 nN / 3 min. Quantitative statistics of RFI and cellular responding ratio were shown in (*D*) and (*E*), respectively. Asterisks inside the bars showed significant difference of this bar to the baseline '1'. *, $p < 0.05$, **, $p < 0.01$. n = 5-6.

Figure S8

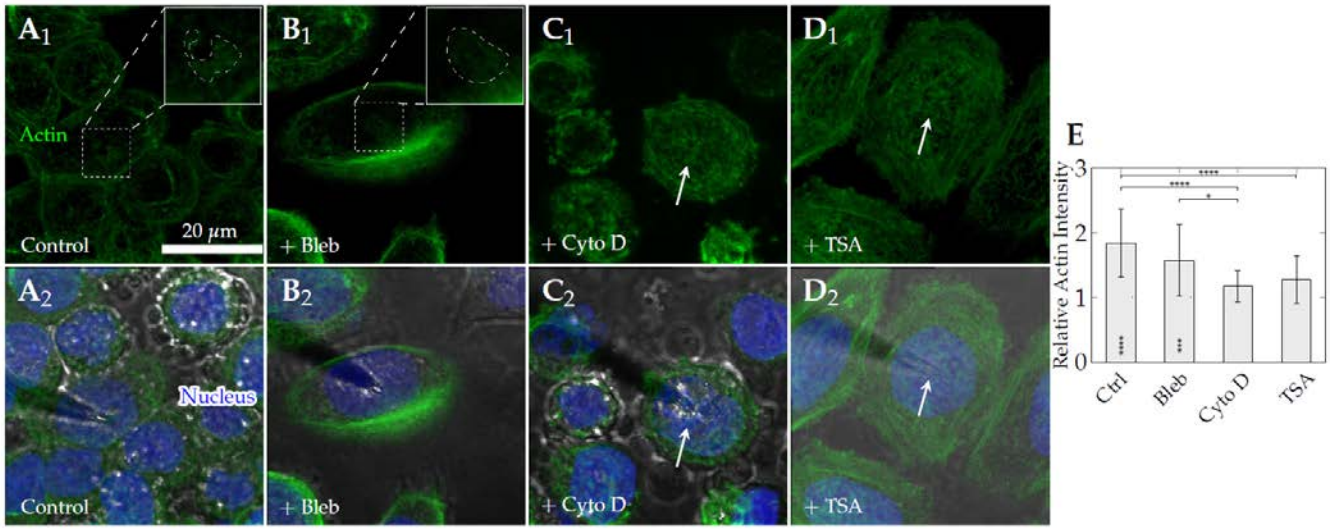

Figure S8. Alteration of local actin intensity enhancement by blocking the key molecules of myosin contraction, actin polymerization and histone deacetylase inhibiting induced chromatin decondensation using respective inhibitors for HeLa cells. Local actin intensity enhancement at the point loading site was captured with 3D reconstruction right after (<2 s) loading the cell using the microneedle (about 1 min for reconstruction). (A_1-D_1) depicted the cell responses without drug treatment or when treating the cell using 15 μM Bleb for 20 min, 15 μM Cyto D for 20 min, and 100 nM TSA for 24 h, respectively. Dashed square boxes in (A_1-B_1) depicted the region of local actin intensity enhancement as magnified in inserts (the region with local actin intensity enhancement was embraced by an irregular dashed contour, and the central hole of which indicated the site occupied by the needle). White arrows indicated the loading site in (*C*-*D*). Bright field and stained nucleus were shown in (A_2-D_2). (*E*) The RFI normalized to the background was calculated as the mean ± SD in each case and compared among distinct cases. Asterisks inside columns showed significant differences among groups to baseline '1'. *, $p < 0.05$, ***, $p < 0.001$, ****, $p < 0.0001$. n = 20-31 and from 2-3 repeats.

Figure S9

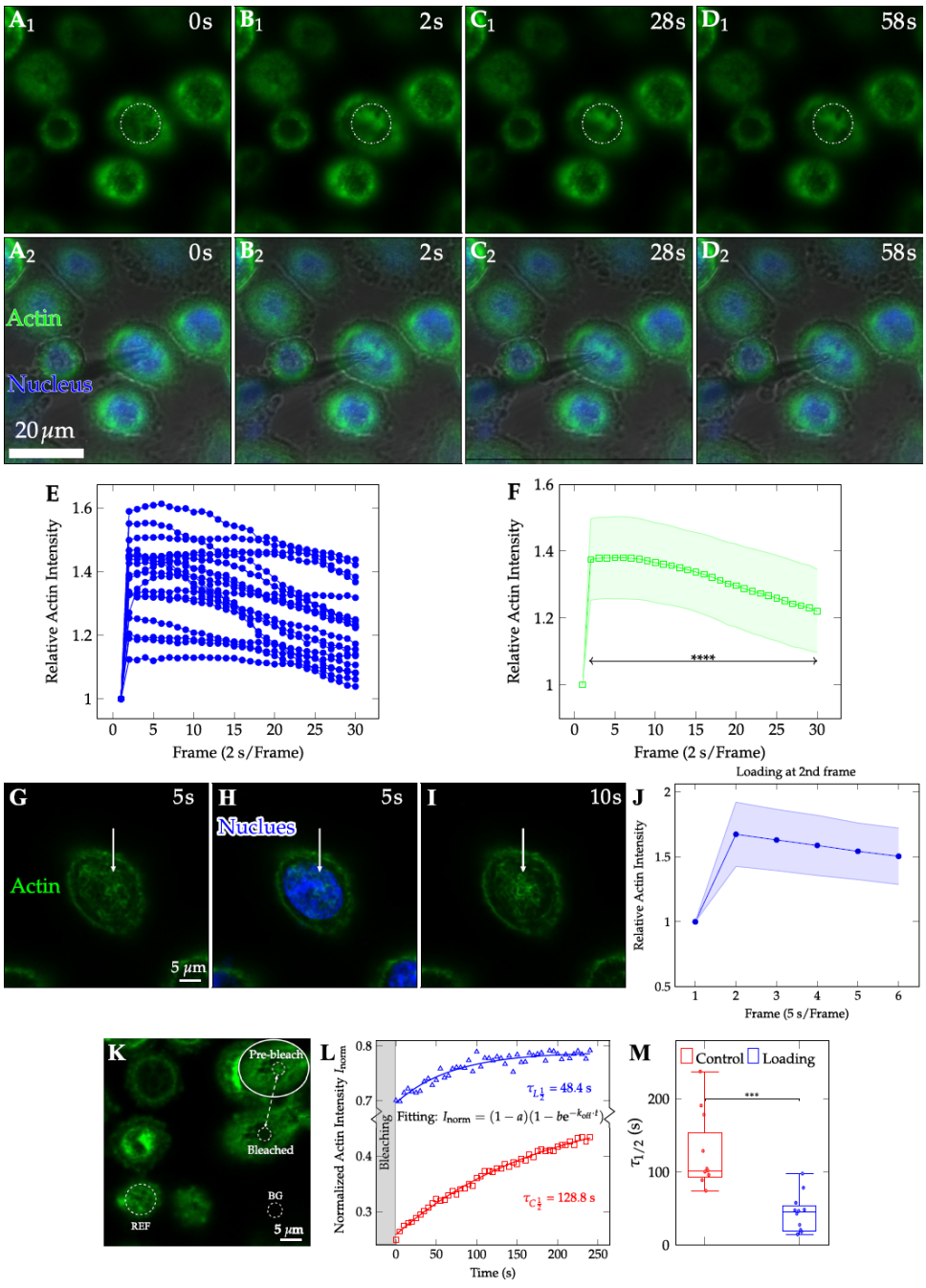

Figure S9. Loading dynamics of local actin (*green*) intensity enhancement at the point loading site of HeLa cell using microneedle assay. (*A-D*) denoted the serial images of actin (*green*) fluorescent intensity in 1 min without 3D reconstruction, the interval time is 2 s and 30 frames in total. The needle was in hover at the first frame (first 2 s) as in (A_1 and A_2) and then loaded on the top of the nucleus (*blue*) at the second frame (4 s) as in (B_1 and B_2). The loaded region was annotated as white dashed circles. (*E-F*) Time evolution of mean RFI that were quantified from (*A-D*) and normalized to the different value between the background and the first frame were shown for each cell (*E*) or accumulative mean ± SD of all cells (*F*). Asterisks showed significant difference among 2nd-30th frame to the first one (n = 20). (*G-J*) Confirmation of fast actin reorganization dynamics upon point loading. Actin reorganization dynamics was evaluated by a fast '3DR'+'TS' mode for

the upper half of the cell only. 3D reconstruction of a cell only took 5 s in this setting. The microneedle was in hovering at the first frame (*G* and *H*) and then loaded at the second frame (*I*). The time course of fluorescence intensity was quantified in (*J*). *White arrows* indicated the point loading site. (K-M) Actin recovery dynamics upon FRAP tests. The photobleached area was set as a circle with the diameter of 2.5 μm (*K*). Typical data of actin recovery dynamics in the absence (*red*) and the presence of point loading (*blue*) were shown (*points*) with respective fitted curves (*lines*) (*L*). The fluorescence intensity of bleached areas was normalized by a reference area (*REF*) and a background (*BG*) area. Statistic data of the half-life estimated from fitted curves ($\tau_{1/2} = \ln 2/k_{off}$) were shown in (*M*). ***, $p < 0.001$, ****, $p < 0.0001$.

Figure S10

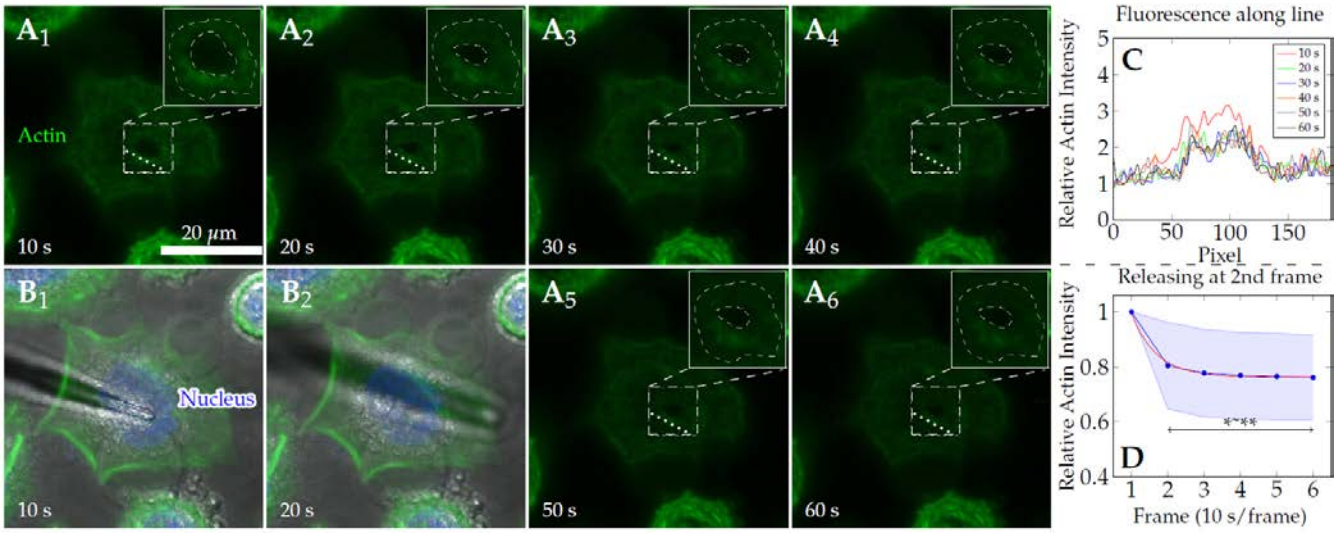

Figure S10. Recovery dynamics of local actin fluorescence intensity of HeLa cells after removing the microneedle from the loading site. (A_1–A_6) denoted the serial images of actin (*green*) fluorescent intensity in 1 min with 3D reconstruction every 10 s (thus 6 frames in total). The needle had been loading on the nucleus for 2 min 50 s before collecting fluorescence. After finishing the first frame, the needle was lifted apart and kept in hover as in (B_1 and B_2). Dashed square boxes in (A_1–A_6) depicted the region of local actin intensity enhancement as magnified in inserts (the region of local actin intensity enhancement was embraced by irregular dashed contour). (*C*) Spatiotemporal distribution of RFI along the white dotted line in dashed boxes in (A_1–A_6). (*D*) Evolution of mean RFI ± SD (*blue*) in the entire dashed regions in inserts. The mean RFI data was then fitted using an empirical equation, $I(t) = I_{base} + \exp(-t/\tau_0)$ (*red* line), in which I_{base} denotes the baseline fluorescence and τ_0 the characteristic time. Half-life time of RFI decay was obtained from curve fitting as $\tau_{1/2} = t_1 + \tau_0 \ln 2 =$ 14.8 s when $t_1 =$10 s. Asterisks showed significant difference among 2-6 frames to the first one. *, $p < 0.05$, **, $p < 0.01$. $n =$ 10.

Figure S11

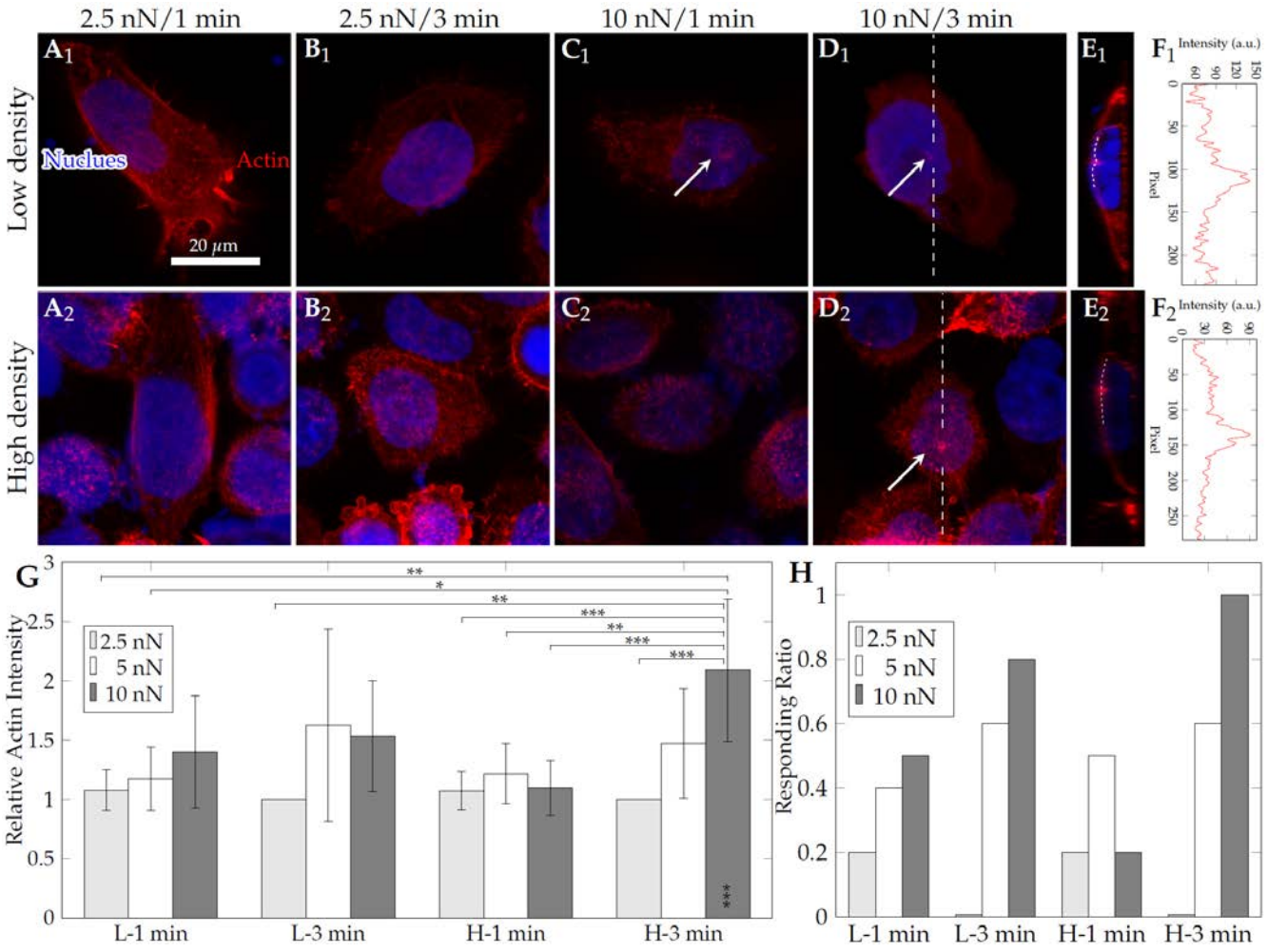

Figure S11. Cell density dependence of local actin intensity enhancement of HeLa cells upon AFM assay. Cells seeded in low density meant each cell was isolated without direct communication with other cells. Here force values of 2.5, 5 and 10 nN and loading duration of 1 min and 3 min were applied. (A_1-D_1) depicted the cell responses after loading in 2.5 nN/1 min, 5 nN/3 min, 10 nN/1 min and 10 nN/3 min for cells seeded in low density ('L-'). The counterparts for cells seeded in high density ('H-') were shown in (A_2-D_2). Images for 5 nN/(1, 3) min were not shown for clarity. Typical cross-sections for local actin intensity increase sites as labeled using white dashed line and white arrow in (*C-D*) were shown in (*E*) and corresponding fluorescence intensity along the dashed white dotted line in membrane were shown in (*F*). The actin intensity peak revealed local actin intensity enhancement at the point loading site. Quantified comparisons of RFI and responding ratio between low and high density seeded cells were shown in (*G* and *H*), respectively. Asterisks inside the last bar of (*G*) showed significant difference of this bar to baseline '1'. *, $p < 0.05$, **, $p < 0.01$, ***, $p < 0.001$. n = 5-6 for each condition.

Figure S12

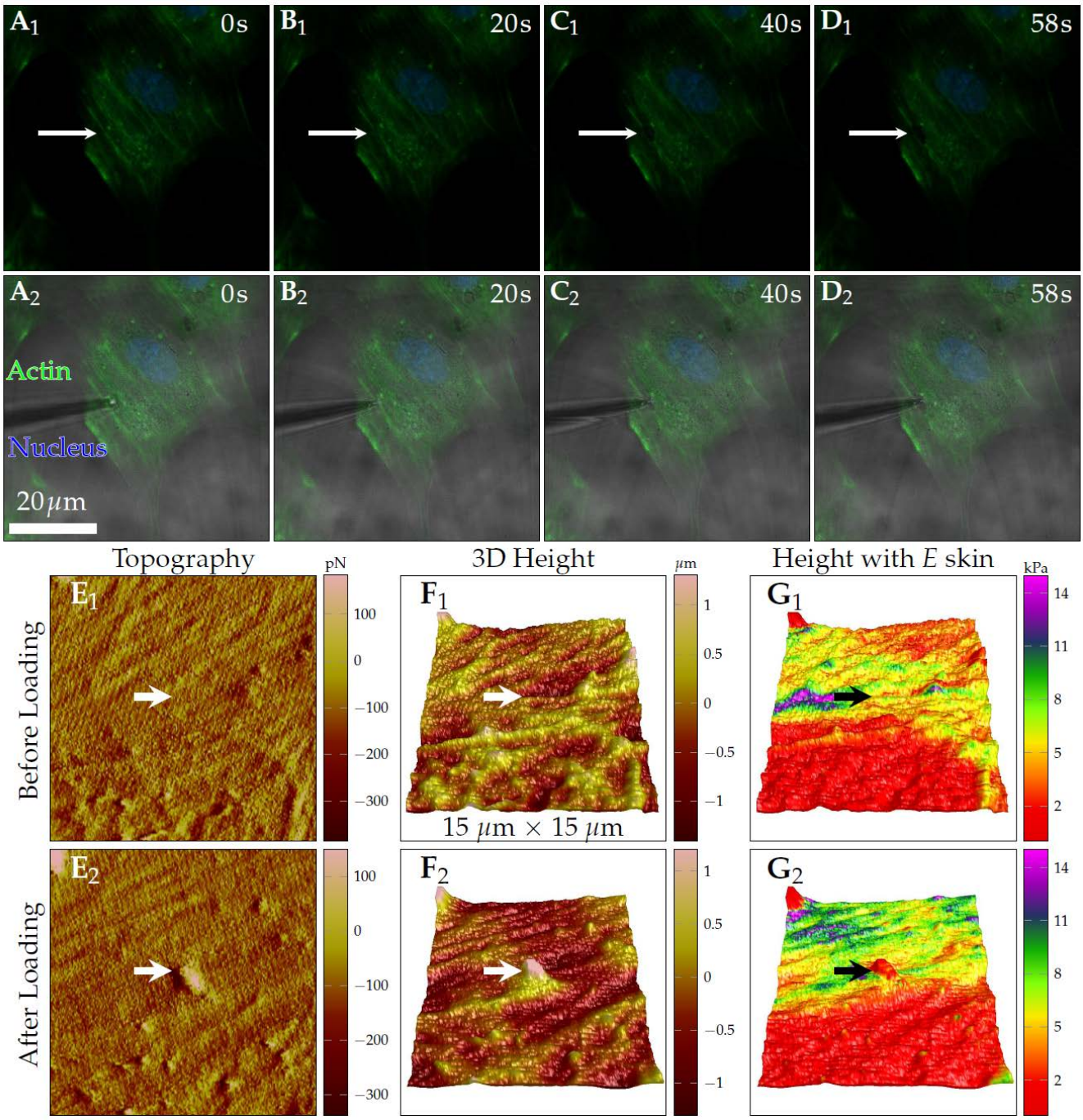

Figure S12. Stress fibers were disrupted when point loading at the cell periphery of HUVEC. (*A-D*) Disruption of stress fiber when loading at cell periphery using microneedle. After loading for about 20 s (*B*), pronounced disruption of stress fiber was captured. (*E-G*) When loading cell periphery using AFM at 5 nN / 3 min, disruption of stress fiber could be captured occasionally as in (*E* and *F*) with *white* arrows labelled. The sharp decrease of stiffness at the loading point (indicated as the *black* arrow in (*G*) also captured the disruption of stress fiber. (E_1-G_1) Scanning for the first time and (E_2-G_2) scanning for the second time, a similar protocol in Figs. 1 and 2.

Figure S13

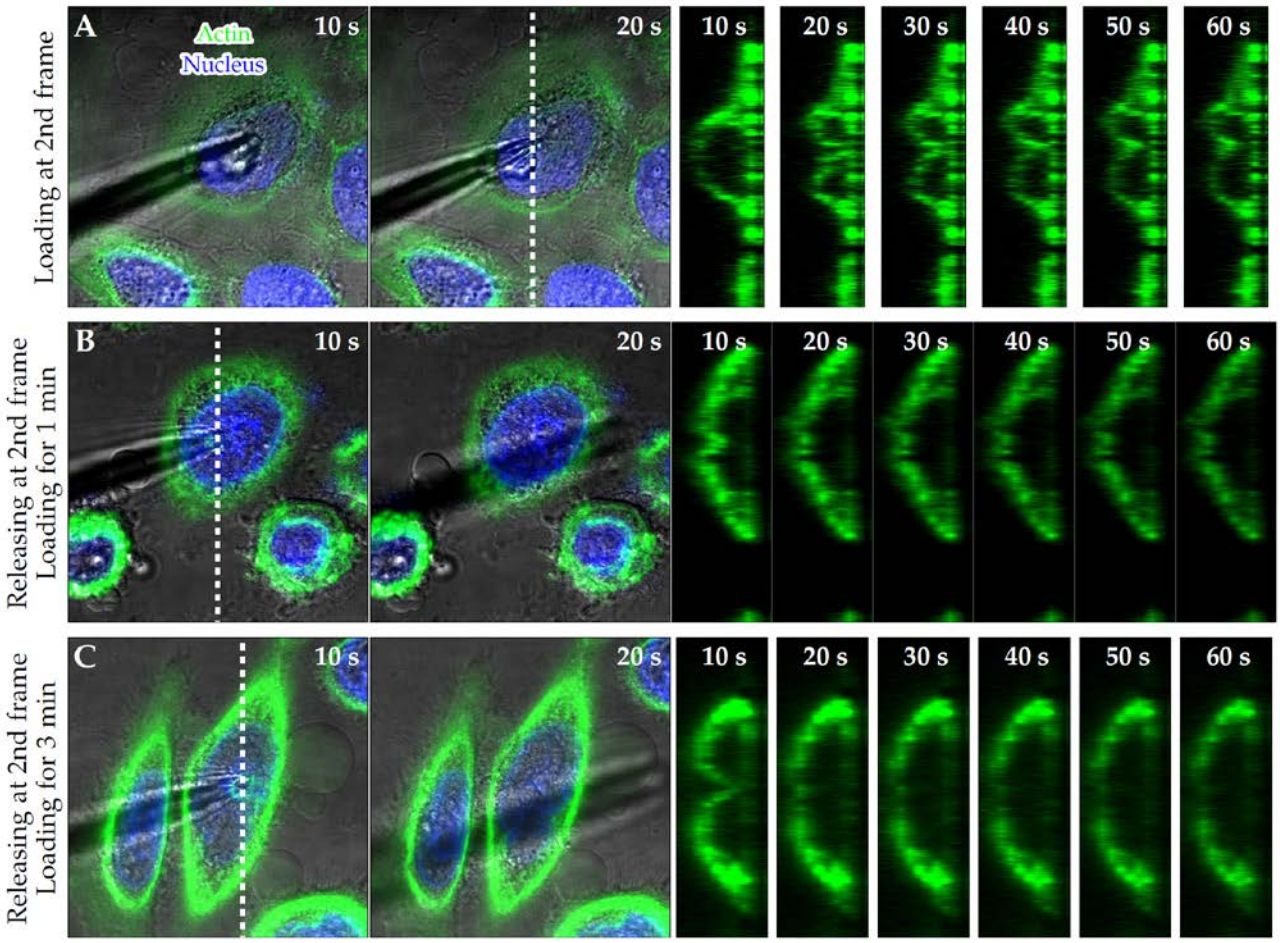

Figure S13. Cellular viscous effect under microneedle loading. Recovery dynamics of cellular deformation in the processes of loading (*A*), and unloading after 1- (*B*) or 3-min (*C*) loading.